



Cross Section of Electron - Off-Shell Nucleon Interaction

K.Sh. Egiyan, M.M. Sargsyan

Yerevan Physics Institute, Yerevan, Armenia

Abstract

The results of theoretical calculations of the electron-bound nucleon interaction cross section (σ_{eN}) are given for four theoretical approaches. It is shown that there are significant differences between predictions of these methods, especially for the deeply bound (high internal momentum, high removing energy) nucleons. To test these predictions experimentally we study of cross sections obtained for two primary energies or for bound proton and neutron. These ratios will be insensitive to the nuclear spectral function as well as to the off-shell modifications of the bound nucleon form-factors if every pair of measurements are made for the same values of energy and momentum-transfers, removal energy, internal and final momenta of the struck nucleon. It is shown that dependences of the discussed ratios on various kinematical parameters are significantly different in different approaches and can be used to distinguish the theoretical models used.

1. Introduction

The cross section for unpolarized electron-nucleus scattering with coincident detection the final state electron and the nucleon can be expressed /1/ via the four nuclear structure functions W_i

$$\frac{d^3\sigma}{d^3\vec{p}_e' d^3\vec{p}_f} = p_f E_f \cdot \sigma_M \cdot \frac{Q^2}{2\bar{q}^2 \epsilon} \cdot [W_T + 2\epsilon \cdot W_L - \epsilon \cdot W_{TT} \cdot \cos 2\phi - (\epsilon(1+\epsilon) \cdot \frac{Q^2}{\bar{q}^2})^{1/2} \cdot W_{LT} \cdot \cos \phi] \quad (1)$$

where $\sigma_M = [\frac{2\alpha E_e' \cos \theta_e' / 2}{Q^2}]^2$ is the Mott cross section, $\epsilon = [1 + \frac{2\bar{q}^2}{Q^2} \cdot \tan^2 \frac{\theta_e'}{2}]^{-1}$ is the virtual photon polarization parameter; $\alpha = 1/137$; Q^2 and \bar{q}^2 are the four and three momentum transfers, θ_e' and \vec{p}_e' are the angle and momentum of scattered electron; E_f and \vec{p}_f are total energy and momentum of the nucleon in the final state; ϕ is the angle between the plane of the scattered electron and the secondary nucleon.

If we consider the electron-nucleus scattering in terms of scattering from bound nucleons and assume that the dependence of all nuclear structure functions in (1) on the bound

nucleon kinematical parameters are the same, then in the framework of the Impulse Approximation this cross section simplifies to a term characterizing the interaction of virtual photon with a bound nucleon, convoluted with a term characterizing the momentum and removal energy distributions of these nucleons. In a nonrelativistic approximation, this factorization is well known [2], and the cross section (1) can be presented as follows:

$$\frac{d^3\sigma}{dE_{e'} d\Omega_{e'} d^3\vec{p}_f} = \sigma_{eN} \cdot S(E_i, \vec{p}_i) \quad (2)$$

where $S(E_i, \vec{p}_i)$ is a nuclear spectral function and indicates the probability to find a nucleon with momentum \vec{p}_i and separation energy E_i the in nucleus. σ_{eN} is the cross section for the interaction of an electron with the bound nucleon, without flux and recoil factors.

In the relativistic description, the factorization (2) is still valid. However the spectral function is different and depends on relativistic kinematical parameters of the bound nucleon (see below).

For the extraction of the information on the nuclear spectral function, the precise knowledge of σ_{eN} is necessary. Such knowledge is important also for the investigation of the modifications of the bound nucleon due to the nuclear environment.

In this work, the first results of theoretical calculations (without contribution of the final state interaction and meson exchange current) in four off-shell approaches are presented. To experimentally test of the predictions of the different approaches, the two ratios of cross sections are considered. Due to the choice of special kinematical conditions for the measurements, these ratios do not depend on the nuclear response [3].

2. Theoretical Approaches for σ_{eN} Calculations

The cross section σ_{eN} will be considered in the four approaches for the quasielastic kinematical region of the $(e, e'p)$ reaction.

2.1. Theoretical Approaches in the "Minimal Relativistic" Impulse Approximation

In this class of Impulse Approximations [4,5], relativistic kinematics were used, but the space-time development of processes correspond to the nonrelativistic representation. To illustrate the origin of nonrelativistic nature of these approaches, let us decompose the invariant Feynman diagram of the $A(e, e'N)A-1$ reaction into the sum of two noncovariant "old fashioned" diagrams (Fig.1). The amplitudes of these diagrams are proportional to the corresponding energy denominators which are

$$\Delta H_a = E_N + E_{A-1} - E_A \quad (3a)$$

$$\Delta H_b = E_{N'} + E_N - q_0 \quad (3b)$$

where E_i are the total energies and q_0 is the energy of virtual photon, (A-1) is the residual system which consist of the (A-1) nucleons.

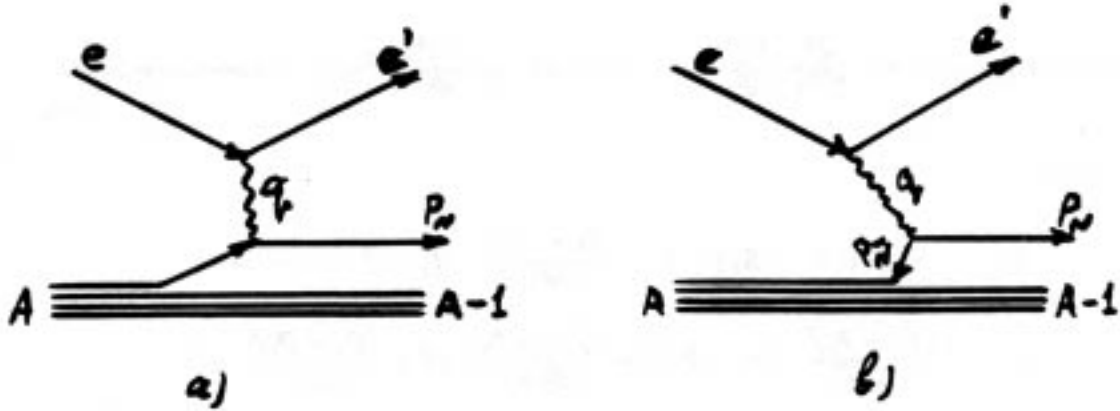


Fig.1

From eq.(3) follows that at the small values of p_N and q_0 , $\Delta H_a \sim p^2/m \rightarrow 0$, while $\Delta H_b \sim 2m$. Therefore, the contribution of the diagram Fig.1b can be neglected which leads to the nonrelativistic IA space-time representation.

However, at high momentum p_N and high energy of virtual photon, the value of ΔH_b can be commensurable with ΔH_a , and the vacuum polarization term (Fig.1b) cannot be neglected. In approaches that neglect this term the problem of the enhancement of the off-shellness has to be solved, because the nonconservation of the invariant energy at the vertex of interaction (off-shellness)

$$\Delta = (P_N + P_{A-1} + q)^2 - (P_A + q)^2 = (M^*)^2 - M_A^2 + 2q_0 \cdot \Delta H_a \quad (4)$$

increases with q_0 if $p_N \neq 0$ (in (4) M^* is the effective mass of $(P_N + P_{A-1})$ system). The real estimation of such effects is often done in the following approximations:

A. The σ^{1GG} approximation [4]. This approximation based on two general assumptions:

i) Current conservation takes place for bound nucleons which allows to express the longitudinal current component via the nucleon charge density:

$$J_i^q = (q_0/q) \cdot J_i^0 \quad (5)$$

where the on-shell expression for charge density is used.

ii) In the description of the off-shell nucleon spinors the following effective energy have been used:

$$E_i^* = (M^2 + p_i^2)^{1/2} = [M^2 + (\vec{p}_f - \vec{q})^2]^{1/2} \quad (6)$$

With these assumptions:

$$\sigma_{eN}^{1CC}(Q^2, \nu, \vec{p}_i, E_i) = \sigma_M \cdot \frac{Q^2}{2\vec{q}^2 \epsilon} \cdot \left[\frac{2Q^2}{\vec{q}^2} \epsilon \cdot \omega_L + \omega_T + (\epsilon(1+\epsilon) \cdot \frac{2Q^2}{\vec{q}^2})^{1/2} \cdot \omega_{LT} \cdot \cos\phi + \epsilon \cdot \omega_{TT} \cdot \cos 2\phi \right] \quad (7)$$

where

$$\begin{aligned} \omega_L &= \frac{1}{4E_i^* E_f} \left((E_i^* + E_f)^2 [F_1^2 - \frac{(P_f - P_i)^2}{4M^2} \cdot F_2^2] - \vec{q}^2 \cdot (F_1 + F_2)^2 \right) \\ \omega_T &= -\frac{(P_f - P_i)^2}{2E_i^* E_f} \cdot (F_1 + F_2)^2 + \frac{\vec{p}_f^2 \cdot \sin^2 \theta_{qf}}{E_i^* E_f} [F_1^2 - \frac{(P_f - P_i)^2}{4M^2} \cdot F_2^2] \\ \omega_{TL} &= -\frac{p_f \cdot \sin \theta_{qf}}{E_i^* E_f} \cdot (E_i^* + E_f) \cdot [F_1^2 - \frac{(P_f - P_i)^2}{4M^2} \cdot F_2^2] \\ \omega_{TT} &= \frac{\vec{p}_f^2 \cdot \sin^2 \theta_{qf}}{E_i^* E_f} [F_1^2 - \frac{(P_f - P_i)^2}{4M^2} \cdot F_2^2] \end{aligned} \quad (8)$$

In equations (8), θ_{qf} is the angle between the vectors of the knock-out nucleon and the virtual photon; P_f and P_i are the four momenta of knockout and bound nucleons; $F_1(Q^2)$ and $F_2(Q^2)$ are the Dirac form-factors of the bound nucleons.

B. The σ^S approximation [5]. Here, the general assumptions made are:

i) At the vertex of the γ^*N interaction the current conservation is restored by including the additional term proportional to q_μ :

$$J_i^\mu = J_\sigma^\mu + q_\mu U_i(q) \quad (9)$$

where J_σ^μ is the current for free nucleons and $U_i(q)$ is an unknown function which can be obtained from current conservation $(q_\mu J_i^\mu) = 0$, i.e. $U = (q_\mu J_\sigma^\mu)/q_\mu^2$.

ii) For the off-shell nucleon the effective mass m^* has been introduced:

$$m^* = \sqrt{E_i^2 - p_i^2} = \sqrt{(E_f - \nu)^2 - (\vec{p}_f - \vec{q})^2} \quad (10)$$

With these assumptions;

$$\begin{aligned}
\sigma_{eN}^S &= \frac{\alpha^2}{Q^4} \cdot \frac{E_e}{E_{e'}} \cdot \frac{1}{E_i^* E_f} \cdot \frac{1}{[1 + Q^2/(M + M^*)^2]} \times \\
&\times \left([4(P_e P_f) \cdot (P_{e'} P_f) - M^2 \cdot Q^2] \cdot [F_1 - \frac{Q^2}{4M^2} \cdot F_2]^2 + \right. \\
&\left. + \frac{Q^2}{(M + M^*)^2} \cdot [4(P_e P_f) \cdot (P_{e'} P_f) + 2(q_\mu P_f)^2 + M^2 \cdot Q^2] (F_1 + F_2)^2 \right)
\end{aligned} \tag{11}$$

where P_e and $P_{e'}$ are four momenta of the incident and scattered electrons and $E_i^* = (M^{*2} + p_i^2)^{1/2}$.

C. The σ^{PIN} approximation. This approximation neglects off-shell effects. The momenta of all incident particles are obtained from the momenta of the final (detected) particles.

$$\begin{aligned}
\sigma_{eN}^F &= \frac{\alpha^2 E_{e'}}{Q^4 \cdot E_e \cdot (E_f - q_0) E_f} \cdot \left([4(P_{e'} P_f)^2 - 2(P_{e'} P_f) Q^2 - M^2 Q^2] \right. \\
&\left. \times [F_1^2 + \frac{Q^2}{4M^2} F_2^2] + \frac{1}{2} Q^4 (F_1 + F_2)^2 \right)
\end{aligned} \tag{12}$$

As can be seen, all these approximations use fully relativistic kinematics; the main differences originate from the treatment of current conservation for off-shell nucleons.

2.2 Relativistic Light Cone Approximation

Now let us consider the diagrams in Fig.1 in the Light Cone (LC) reference frame [6,7], which is characterized by four-momenta

$$P^\mu(p_+, p_-, \vec{p}_\perp) \tag{13}$$

with

$$p_+ = E + p_z = \sqrt{m^2 + p_\perp^2} + p_z \tag{13'}$$

$$p_- = E - p_z = \sqrt{m^2 + p_\perp^2} - p_z \tag{13''}$$

where (-) and (t) components are conserved for all vertexes, and particles are taken on their mass-shell [7].

For the interaction of virtual photon with spinless particles the number of diagrams is still two. One of these diagram (vacuum diagram in Fig.1b) vanishes due to the nonconservation of the (-) component ($q_- - p_{N-} - p_{N-} < 0$, because $q_- = \nu - \sqrt{Q^2 + \nu^2} < 0$ and

$p_{N-} + p_{N+} > 0$). Consequently, only the diagram in Fig.1a should be taken into account, for which the energy denominator is

$$\Delta H_a = \frac{A \cdot (m^2 + p_t^2)}{\alpha \cdot p_{A-}} + P_{(A-1)+} - \frac{M_A^2}{p_{A-}} \quad (14)$$

where $\alpha = A \cdot p_{N-} / p_{A-}$ is the momentum fraction carried by constituent nucleon.

Note, that in this approximation the nonconservation of invariant energy at the $\gamma^* N$ amplitude does not increase with transferred energy (see (4)). Indeed, at the $\gamma^* N$ vertex, the energy nonconservation is

$$\Delta = (P_N + P_{A-1} + q)^2 - (P_A + q)^2 = (M^*)^2 - M_A^2 + (q_0 - q_s) \cdot \frac{M^{*2} - M_A^2}{M_A} \quad (15)$$

which does not increase with q_0 , since $q_0 - q_s = q_0 - \sqrt{Q^2 + q_s^2}$.

It should be pointed out that in LC approximation the spectral function will depend on the Light-Cone variables $(\alpha, \vec{p}_t, p_{A-1+})$ (see (14), [6]) and

$$\frac{d^3 \sigma}{dE_e d\Omega_e d^3 \vec{p}_f} = K \cdot \sigma_{eN} \cdot P(\alpha, \vec{p}_t, p_{(A-1)+}) \quad (16)$$

i) For calculations of the σ_{eN} in LC approximation the problem of uncertainties of the bound nucleon current must be solved. The general assumption is that the current conservation takes place for off-shell nucleons. Since for the transvers and "n" components of the bound nucleon current the free nucleon current components can be used, the requirement of current conservation allows one to obtain the unknown longitudinal component of bound nucleon current:

$$J_{N+} = -\frac{q_+}{q_-} \cdot J_{N-} \quad (17)$$

However, in actual σ_{eN} calculations, the spin of the bound nucleon must be taken into account, which results in one more diagram, the so called contact diagram. One can show that for this diagram the contribution of J_{N-} component is absent ("Good" component) [7,8]. As for the transfer component, numerical calculations indicate [6] that its contribution do not exceed 1÷2% in the $\approx 1(\text{GeV}/c)^2$ momentum-transfer range. So, the contribution of the contact diagram, which is due to the J_{N+} component only, is effectively already taken into account by using (17).

ii) The off-shell continuation of the "+" component of the initial nucleon momentum is obtained by assuming that:

$$p_+ = (P_A - P_{A-1})_+ = \frac{\vec{m}^2 + p_t^2}{p_-} \quad (18)$$

where [6]

$$m^2 - \bar{m}^2 = \alpha \cdot \left(\frac{m^2 + p_f^2}{\alpha} + \frac{m_{A-1}^2 + p_i^2}{A - \alpha} - \frac{m_A^2}{A} \right) \quad (19)$$

Thus, in LC approximation, σ_{eN} will be calculated using the general expression (7) with new elementary structure functions [9]:

$$\begin{aligned} \omega_L &= \frac{q^2}{E_f \cdot m} \cdot \left\{ F_{1N}^2(Q^2) \cdot \frac{\alpha_f \cdot \alpha}{\alpha_q^2} - F_{1N}(Q^2) \cdot F_{2N}(Q^2) \cdot \frac{\alpha_f - \alpha}{2\alpha_q} + \right. \\ &\quad \left. + \frac{F_{2N}^2(Q^2)}{4m^2} \cdot \left[\frac{-1}{2} \cdot (m^2 + (p_f p)) + Q^2 \cdot \frac{\alpha_f \cdot \alpha}{\alpha_q^2} + (pq) \cdot \frac{\alpha_f}{\alpha_q} + (p_f q) \cdot \frac{\alpha}{\alpha_q} \right] \right\} \\ \omega_T &= \frac{1}{E_f m} \cdot \left\{ F_{1N}^2(Q^2) \cdot (p_f^y p^y + (p_f p) - m^2) - F_{1N}(Q^2) \cdot F_{2N}(Q^2) \cdot (p_f - p; q) + \right. \\ &\quad \left. + \frac{F_{2N}^2(Q^2)}{4m^2} \cdot [Q^2 \cdot ((p_f^y p^y + (p_f p) - m^2) - 2 \cdot (pq) \cdot (p_f q))] \right\} \\ \omega_{TL} &= \frac{|\bar{q}| \cdot p_f^y}{E_f \cdot m} \cdot \left\{ F_{1N}^2(Q^2) \cdot \frac{\alpha_f + \alpha}{\alpha_q} + \frac{F_{2N}^2(Q^2)}{4m^2} \cdot [Q^2 \cdot \frac{\alpha_f + \alpha}{\alpha_q} + (pq) + (p_f q)] \right\} \\ \omega_{TT} &= \frac{p^y \cdot p_f^y}{E_f \cdot m} \cdot \left\{ F_{1N}^2(Q^2) + Q^2 \cdot \frac{F_{2N}^2(Q^2)}{4m^2} \right\} \end{aligned} \quad (20)$$

where $\alpha_q = A \cdot (q_0 - q_3) / P_{A-}$ ($q_3 = |\bar{q}|$), $\alpha_f = \alpha + \alpha_q$, $p_f^y = p^y = p \cdot \sin(\theta_{qf})$, and

$$\begin{aligned} (p_f p) &= p_f^\mu (p_f - q)_\mu + \frac{1}{2} \cdot \frac{(m^2 - \bar{m}^2)}{\alpha} \cdot \alpha_f \\ (pq) &= (p_f - q)^\mu q_\mu + \frac{1}{2} \cdot \frac{(m^2 - \bar{m}^2)}{\alpha} \cdot \alpha_q \\ (p_f q) &= -\frac{Q^2}{2} + \frac{1}{2} \cdot (m^2 - \bar{m}^2) \end{aligned} \quad (21)$$

4. Numerical Calculations of σ_{eN}

The goal of this work is to find out the characteristics of σ_{eN} for an internuclear momentum range from $pp_{\text{ Fermi}}$ to $\approx 0.7 \text{ GeV}/c$. Since there are reliable theoretical [6,10] and experimental [11] statements that short-range two-nucleon correlations are responsible

for this momentum region, the calculations will be done using the pair-correlation model of the momentum distribution for which, in nonrelativistic approximation, the sufficiently simple relation between internal momentum and removal energy [10] can be found:

$$\langle E_i \rangle \approx \frac{p_i^2}{2M} \quad (22)$$

in contradiction to the independent behavior of removal energy and momentum in the framework of shell model.

The relativistic (Light-Cone) generalization of (22) is [6]

$$\langle P_{(A-1)+} \rangle \approx M_{A-1} + A \frac{m^2 + p_i^2}{2 - \alpha} \cdot \frac{1}{M_A} \quad (22')$$

$P_{(A-1)+}$ is one of arguments of the spectral function in LC approximation (see (16)).

Using these relations between removal energy and internal momentum, σ_{eN} has been calculated for the quasi-elastic ($e, e'p$) scattering as a function of different kinematical parameters. These results are presented in Fig.2÷4.

In these calculations the following relations between elastic nucleon form-factors were used

$$F_1 = (G_e + \frac{Q^2}{4M^2} G_m) / (1 + \frac{Q^2}{4M^2}); \quad F_2 = (G_m - G_e) / (1 + \frac{Q^2}{4M^2}) \quad (23)$$

where the standard dipole behavior for nucleon magnetic and electric form-factors are assumed:

$$G_{ep} = \frac{G_{mp}}{\mu_p} = \frac{G_{mn}}{\mu_n} = -\frac{G_{en}}{\mu_n} \cdot [1 + 5.6 \cdot \frac{Q^2}{M^2}]^{-1} = \frac{1}{(1 + \frac{Q^2}{0.71})^2} \quad (24)$$

The main conclusions which can be drawn from these data are:

For fixed transfer-momentum :

1. There are big differences between the predictions of the approaches considered.
2. These differences increase with increasing momentum and polar angle of the bound nucleons.
3. Theoretical predictions are significantly different for bound protons and neutrons.

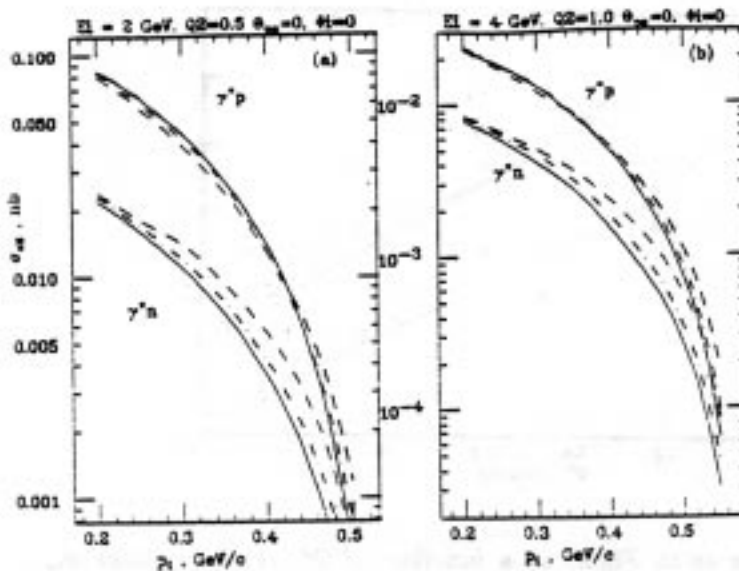


Fig.2 Cross section of electron-bound nucleon elastic scattering as a function of internal momentum p_i , at a) $E_e = 2\text{GeV}$, $Q^2 = 0.5(\text{GeV}/c)^2$, $\theta_{iq} = 0^\circ$, $\phi_{iq} = 0^\circ$, b) $E_e = 4\text{GeV}$, $Q^2 = 1.0(\text{GeV}/c)^2$, $\theta_{iq} = 0^\circ$, $\phi_{iq} = 0^\circ$. The solid, dashed, dash-dotted, dotted curves are the results of σ^{LC} , σ^{CC} , σ^S and σ^{FIN} approximations, respectively. Upper and lower series of curves are for the bound proton and neutron case.

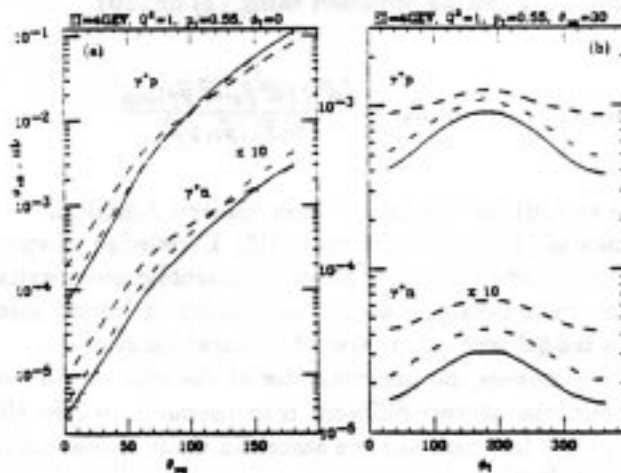


Fig.3 The same as in Fig.1, as a function of polar (a) and azimuthal (b) angles at $E_e = 4\text{GeV}$, $Q^2 = 1.0(\text{GeV}/c)^2$, $p_i = 0.55\text{GeV}/c$ and $\phi_{iq} = 0^\circ$ (a), $\theta_{iq} = 30^\circ$ (b).

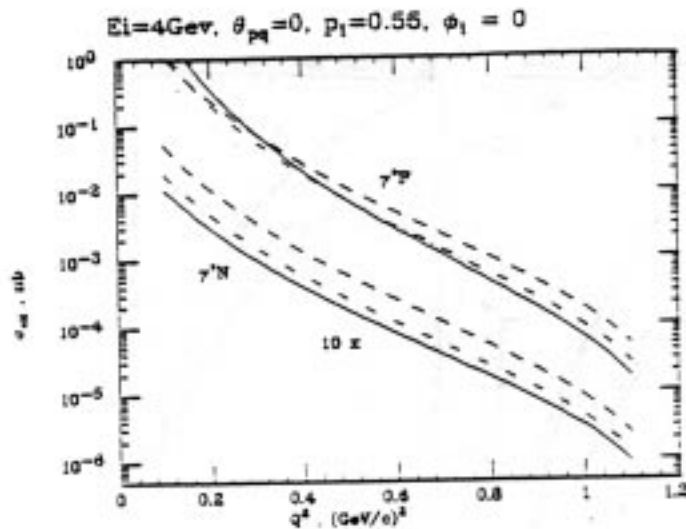


Fig.4 The same as in Fig.1, as a function of Q^2 at $E_e = 4\text{GeV}$, $\theta_{iq} = 0^\circ$, $p_i = 0.55\text{GeV}/c$ and $\phi_{iq} = 0^\circ$.

5. Experimental Methods for Testing the Theoretical Predictions

The direct experimental measurements of σ_{eN} for bound nucleons are impossible due to the nuclear effects. However, it can be obtained using (2) or (16)

$$\sigma_{eN}(E_e, Q^2, \nu, \vec{p}_i, E_i) = \frac{[d^4\sigma/d^3\vec{p}_e d^3\vec{p}_f]_{exp}}{S(E_i, \vec{p}_i, \vec{p}_f)} \quad (25)$$

This is true if one use eq.(16) for the Light-Cone spectral function.

The present (experimental [11] and theoretical [12] knowledge of spectral functions (especially at high internal momenta) does not allow to unambiguously extract the desired value of the σ_{eN} . Therefore, the straightforward estimation of bound nucleon effects in the cross section requires a model free extraction of spectral functions.

One of the methods to suppress the uncertainties of the spectral functions is to construct the ratios of cross sections at two different measurements where all arguments of $S(E_i, \vec{p}_i, \vec{p}_f)$ ($P(\alpha, p_i, P_{(A-1)+})$) function are the same. In these ratios the influence of the spectral function will be cancelled.

We will consider two methods for constructing such ratios.

5.1. Two Energy Method

In this case the ratio R_B of σ_{eN} 's obtained for two incident energies and for the same

values of Q^2 , ν , E_i and \vec{p}_i is considered. In fact this is analogous to a Rosenbluth σ_L/σ_T separation.

$$R_B \equiv \frac{\sigma_{eN}(E_{e1})}{\sigma_{eN}(E_{e2})} = \left(\frac{d^5\sigma(E_{e1})}{d^5\sigma(E_{e2})} \right)_{exp} \quad (26)$$

In R_B , the form-factor modifications of bound nucleons have no contributions because Q^2 (and ν) were assumed equal in the two measurements.

In Fig.5 dependences of R_B to p_i , θ_i , ϕ_i and Q^2 for $E_{e1} = 2GeV$, $E_{e2} = 4GeV$ are presented. All ratios are normalized to R_B^{FIN} (the ratio for the free nucleons).

One can see that there are significant and measurable differences between the predictions of the theoretical approaches considered. In some cases, expected off-shell effects results in more than 100% deviations from the free nucleon predictions.

5.2. Neutron-to-Proton Ratio

The ratio R_N of σ_{eN} 's obtained for the neutron and proton at the same values of incident energy, Q^2 , ν , E_i and \vec{p}_i .

$$R_N \equiv \frac{\sigma_{eN}^n}{\sigma_{eN}^p} = \left(\frac{d^5\sigma^n}{d^5\sigma^p} \right)_{exp} \quad (26)$$

should be independent of the spectral function, if this function is similar for the neutron and proton. In Fig.6 dependences of R_N to p_i , θ_i , ϕ_i and Q^2 for $E_e = 4GeV$ are presented. All ratios are normalized to R_B^{FIN} (the ratio for the free nucleons). One can see that this case also there are significant and measurable differences between the predictions of the theoretical approaches considered.

The principal difference between the two methods discussed is demonstrated in the Q^2 dependences of R_B and R_N (see Fig.5 and Fig.6). For R_B , differences between predictions increase with increasing Q^2 , for R_N vice versa; with increasing Q^2 the predictions of all theoretical models becomes the same.

It should be pointed out that results discussed above were obtained without taking into account effects of final state interaction (FSI) and meson exchange current (MEC). In the kinematical regions where these processes have large contribution, the predictions discussed can be changed significantly. Let us briefly (qualitatively only) consider the expected modifications of the predicted effects in the kinematical regions used, i.e. at $Q^2 \geq 0.5(GeV)^2$ and $x \geq 0.5$ (x is the Bjorken variable for free nucleon) due to the FSI and MEC.

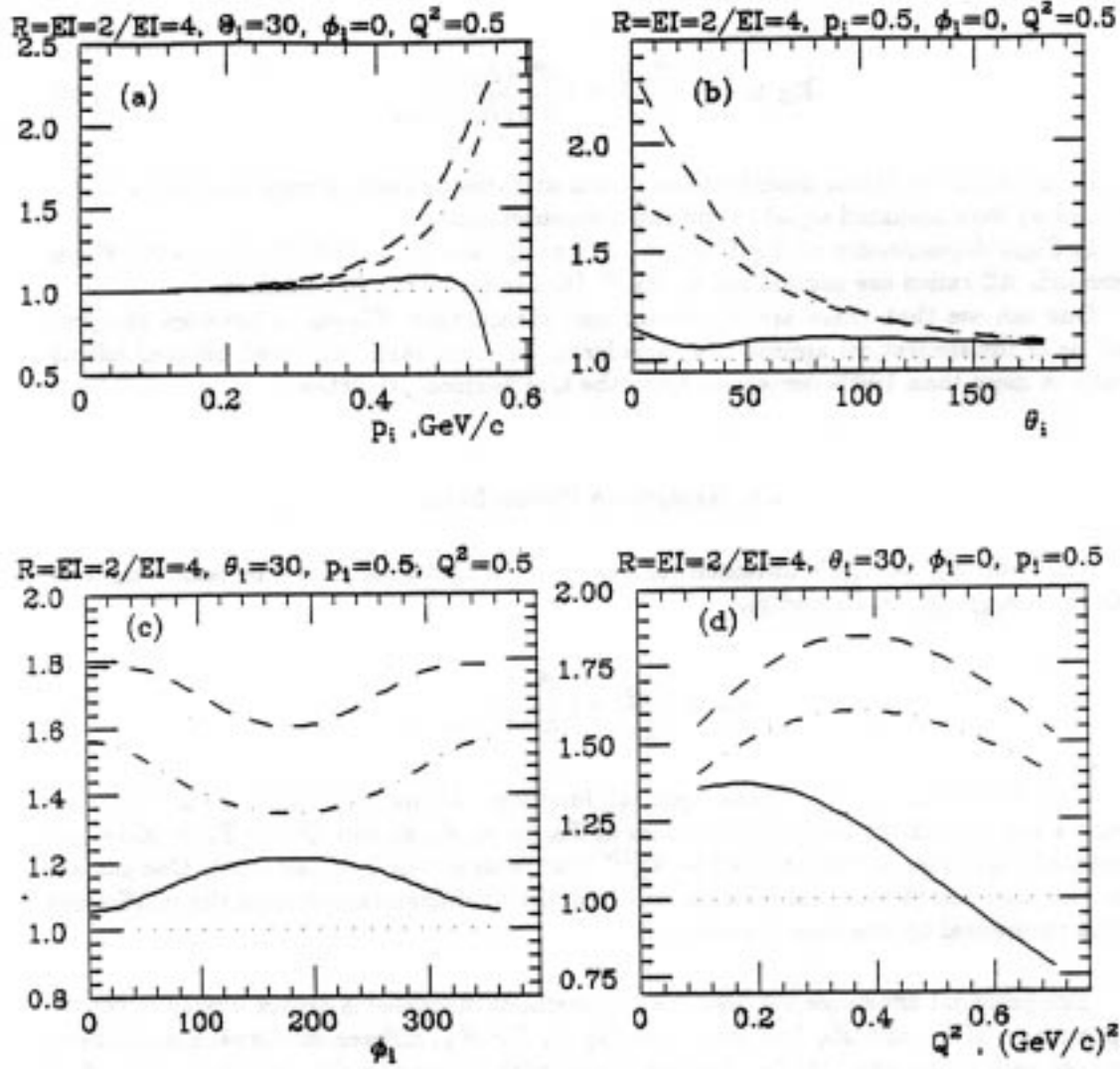


Fig.5 Dependences of the ratio $R_g = \sigma_{eN}(E_{e1})/\sigma_{eN}(E_{e2})$ at $E_{e1} = 2\text{GeV}$, $E_{e2} = 4\text{GeV}$, vs. the (a) internal momentum p_i at $Q^2 = 0.5(\text{GeV}/c)^2$, $\theta_{iq} = 30^\circ$, $\phi_{iq} = 0^\circ$; (b) polar angle θ_{iq} at $p_i = 0.5(\text{GeV})/c$, $Q^2 = 0.5(\text{GeV}/c)^2$, $\phi_{iq} = 0^\circ$; (c) azimuthal angle $\phi_{iq} = 0^\circ$ at $\theta_{iq} = 30^\circ$, $p_i = 0.5(\text{GeV})/c$, $Q^2 = 0.5(\text{GeV}/c)^2$; (d) Q^2 at $\theta_{iq} = 30^\circ$, $\phi_{iq} = 0^\circ$, $p_i = 0.5(\text{GeV})/c$. Solid, dashed, dash-dotted, dotted curves are the results of σ^{LG} , σ^{1GC} , σ^S and σ^{FIN} , approximations, respectively. All ratios calculated for bound proton target.

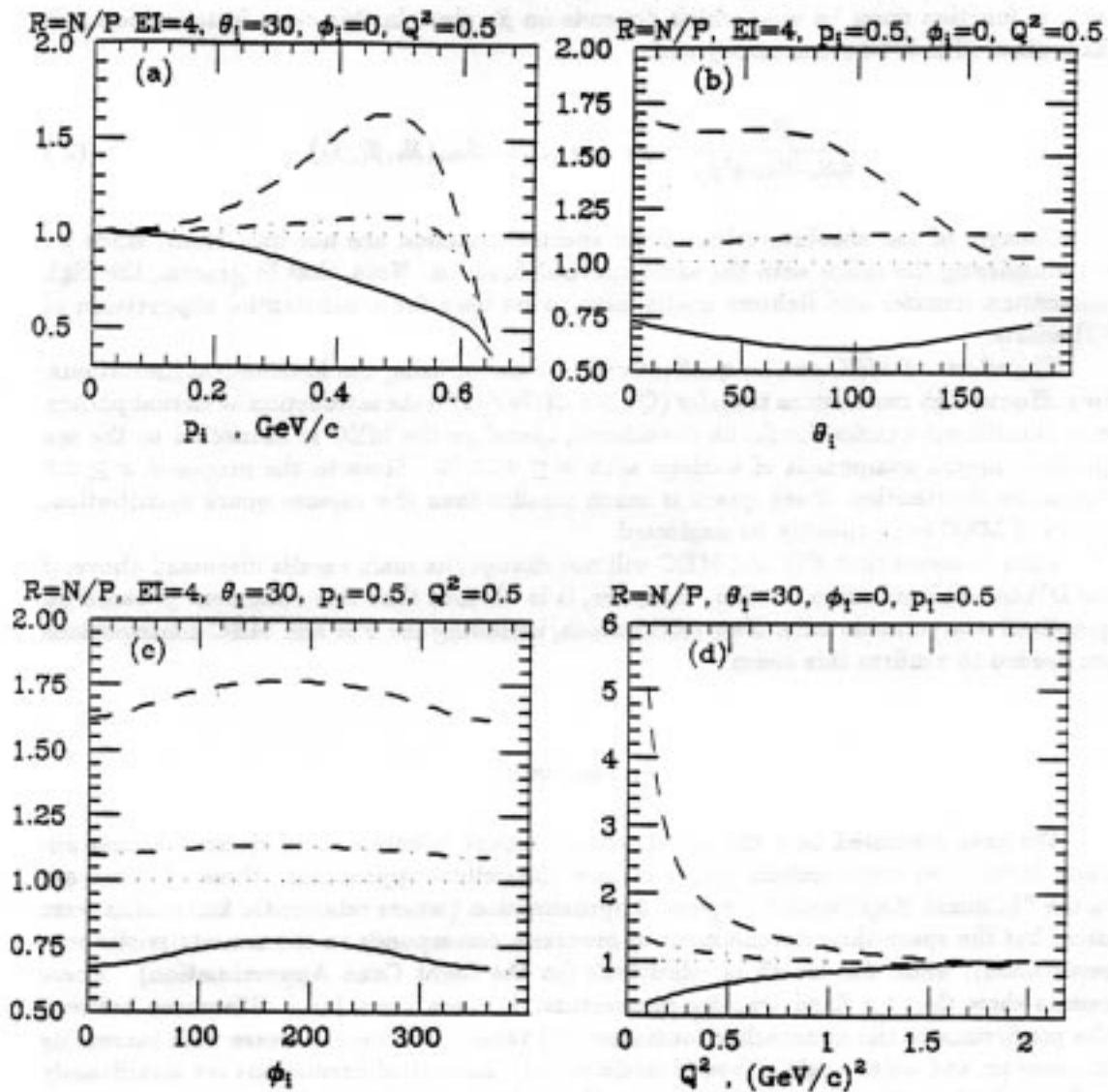


Fig.8 The same as in Fig.6, for the ratios of neutron - proton cross sections at incident electron energy $E_e = 4\text{GeV}$.

The Final State Interaction can result in two important effects: i) the disturbance of the factorization (2), and ii) the change of the spectral function.

In [2] it was shown that to take FSI into account, e.g. in the DWIA, a distorted spectral function must be used which depends on \vec{p}_f also. In this case, factorization still takes place with $\approx 1\div 3\%$ accuracy and

$$\frac{d^6\sigma}{dE_e d\Omega_e d^3\vec{p}_f} = p_f \cdot E_f \cdot \sigma_{eN} \cdot S_{dis}(E_i, \vec{p}_i, \vec{p}_f) \quad (2')$$

Changes of the absolute value of the spectral function are not important, since we are considering the ratios with the same spectral function. Note, that in general, the high momentum transfer and lightest nuclei have to be used for a substantial suppression of FSI effects.

The effects of MEC can be qualitatively estimated using the kinematical limitations: for sufficient high momentum transfer ($Q^2 > 0.5(GeV/c)^2$) the interaction of virtual photon with constituent quarks should be considered, therefore the MEC is connected to the sea quark-antiquark component of nucleon with $x \leq 0.15$ [6]. Since in the proposed $x \geq 0.5$ region the distribution of sea quark is much smaller than the valence quark distribution, effects of MEC can probably be neglected.

Thus, it seems that FSI and MEC will not change the main results discussed above, if the DWIA approximation is valid. However, it is obvious that this statement is based on quantitative arguments only. New calculations, including the FSI and MEC contributions are needed to confirm this claim.

6. Summary

We have presented here the results of theoretical calculations of electron-bound nucleon interaction cross section (σ_{eN}) in four theoretical approaches: three of those are in the "Minimal Relativistic" Impulse Approximation (where relativistic kinematics were used, but the space-time development of processes corresponds to the nonrelativistic representation), while the fourth is relativistic (in the Light Cone Approximation). These results show that for fixed transfer-momentum: i) there are a large differences between the predictions of the approaches considered, ii) these differences increase with increasing momentum and polar angle of bound nucleons, iii) theoretical predictions are significantly different for bound protons and neutrons. Since direct experimental measurements of σ_{eN} for bound nucleons is impossible (due to the nuclear effects) the ratios of cross sections for two different measurements were constructed where all arguments of the nuclear spectral function are the same. In these ratios the influence of the spectral function will cancel. Two methods for constructing such ratios have been considered: the "Two Energy" and "Neutron-to-Proton Ratio" method. It is shown that there are significant measurable differences in predictions of the theoretical approaches. In some cases, expected off-shell effects results in more than 100% deviations from the free nucleon predictions.

Acknowledgments

We wish to thank C. Carlson, L. Frankfurt, B. Mecking, W. Van Orden, A. Radyushkin, E. Smith and M. Strikman for detailed and helpful discussions.

References

1. T. de Forest Jr., *Ann. of Phys.*, 45, 365 (1967).
2. S. Boffi et al., *Nucl. Phys.*, A386, 549 (1982); A435, 696 (1985).
3. G. van der Steenhoven, *Research Program at CEBAF (II)* p. 95, Newport News, VA, 1986.
4. T. de Forest Jr., *Nucl Phys.*, A329 232 (1983).
5. J. Mougey et al., *Nucl. Phys.*, A262, 461 (1976).
6. L.L. Frankfurt, M.I. Strikman, *Phys. Rep.*, v.76, 215 (1981); v.160, 235 (1988).
7. J.B. Kogut., D.E.Soper, *Phys.Rev.*, v.D1, 2901, (1970).
8. J.M. Namyslowski, *PIPNP*, V.14, 1, (1984).
9. L.L. Frankfurt, M.I. Strikman, M.M. Sargsyan, to be published.
10. C.Ciofi degli Atti, S.Simula, L.L.Frankfurt, M.I.Strikman, *Phys.Rev.* C44, R7, (1991).
11. C.Marchand et al., *Phys.ReV.Lett.* 60,1703 (1988).
12. C.Ciofi degli Atti, E.Pace, G.Salme, *Phys.Lett.* 141B, 14 (1984)